CONSTITUTIVE EQUATIONS TO CORRELATE UNIAXIAL CREEP BEHAVIOUR VS STRESS AND TEMPERATURE FOR INCONEL 718

Antonietta Lo Conte
Politecnico di Milano, Department of Mechanical Engineering
Via La Masa 1, 20154 Milano Italy
Phone: +39-0223998223, Fax: +39-0223998282
E-mail: antonietta.loconte@polimi.it

ABSTRACT

The paper presents uniaxial creep tests conducted on Inconel 718 superalloy, reporting and describing the results obtained. The creep strain curves have been examined in different scenarios: by varying the initial applied stress, by varying the initial test temperature, and by considering the orientation of the specimens with respect to the direction of the material processing. Finally, ductility and deformation accumulation rate have been evaluated to highlight the effect of the precipitation anisotropy on the creep behaviour.

Given the complexity of the creep phenomenon, each phase of the creep strain curves of Inconel 718 has been analysed independently, using constitutive models taken from the literature that allow to describe the phenomenon in pure metals and in some alloys.

Keywords: Inconel 718, Creep tests, Constitutive models.

1. INTRODUCTION

Inconel 718 is a precipitation strengthened nickel-based superalloy, widely used for structural components operating at high temperatures in the aviation, aerospace, and power generation industries. The polycrystalline Ni-Fe-base superalloy Inconel 718 derives its excellent high temperature service strength from the disc shaped precipitate γ" (Ni3Nb) and less spherical γ'(Ni3(Ti,Al)) phases, coherently embedded within the γ phase [1,2]. In dealing with the creep phenomenon of Inconel718, two aspects have high importance: the stability of the microstructure and its morphological transformation. As reported in [3], γ' and γ" phases nucleate from the base solution of γ by a replacive ordering of the matrix, and the first clusters of γ' and γ" are formed even after a short annealing time. During the high temperature steady state, when the volume fraction of the precipitates has reached its thermodynamic equilibrium value, the average particle size continues to increase due to the phenomenon called coarsening [4]. Superalloys are characterised by a high-volume fraction of the precipitates; therefore, the mechanisms by which coarsening develops are very complex [5]. The phenomenon whereby large precipitates tend to grow and small ones to dissolve, decreasing the number of particles, is driven by the process of minimising interface energy. Since the lattice parameters of the precipitates are not identical to the lattice parameters of the matrix (γ), there are rearrangements associated with thermal fluctuations of atomic positions that tend to reduce the energy of elastic interaction between the γ phase and the coherent precipitates phases γ" and γ'. Even in the absence of external forces applied, it is necessary to consider local internal stresses given by the phenomenon of lattice misfit [5]. The process of minimising the energy associated with these stresses gives rise to a process of diffusion at the interface between γ phase and precipitates. This process tends to reduce the lattice misfit, causing decrease in the stress value mentioned previously and creating a chemical gradient of equilibrium in a very small region. The speed at which equilibrium is reached depends on several factors, such as the diffusion capacity of the elements and the distance between the precipitates and their volume [6].

When the material remains at high temperature, another important phenomenon called rafting occurs. Precipitates tend to join among each other in blocks of about ten particles, evenly distributed, and are subjected to coalescence. This phenomenon literally corresponds to the formation of precipitate rafts. The phenomenon of rafting becomes more evident and completely anisotropic, at the grain level, when a force is applied during the high temperature steady state. The local orientation of the rafts depends on the direction of the main force applied, respecting the crystalline structure. It also depends on the misfit of the lattice between the γ phase and the precipitates [7, 8].

The need to have materials for increasingly demanding applications, linked to the necessity of using the

material at higher temperatures and stresses, has led to successive developments in the framework of superalloys. In the sixties, Pratt and Whitney developed directional solidification with columnar grain structures for the production of pallets [9]. Unidirectional solidification has had, as further development, the ability to produce a single crystal component where the presence of weak points represented by grain edges is eliminated. Single crystal super alloys are mainly used for the construction of turbine blades, as they ensure greater creep ductility, maintain resistance under higher temperatures, and also have a better fatigue behaviour at high temperatures [10]. However, due to economic reasons, multi-crystal superalloys continue to be used in most high temperature applications [11].

The effects of temperature and stress on the microstructural evolution behaviour of IN718 multi-crystal superalloy has attracted considerable attention over the past several decades. However, most studies only examined the creep behaviour, regardless of the microstructural anisotropy that develops during the phase evolution, thus without accurately addressing the complex servicing environments for components [12].

The paper presents uniaxial creep tests conducted on Inconel 718, reporting and describing the results obtained. The creep strain curves will be examined in different scenarios: by varying the initial applied stress, by varying the initial test temperature, and by considering the orientation of the specimens with respect to the direction of processing of the material. Finally, ductility and deformation accumulation rate will be evaluated to highlight the effect of the precipitation anisotropy on the creep behaviour. Given the complexity of the creep phenomenon, each phase of the creep strain curves of Inconel 718 will be analysed independently using constitutive models taken from the literature that allow to describe the phenomenon in pure metals and in some alloys. Moreover, their possible extension to the material under study will be discussed, defining the parameters for future modelling of creep damage, including transient effects, in components subjected to non-uniform stress and temperature distribution during service, as for example reported in [13] for turbine blade-disk attachment or in modelling thermomechanical fatigue, as reported in [14].

2. MATERIAL

The experimental tests were conducted on the Inconel 718 nickel-based super alloy, supplied in a 150 mm diameter forged bar and subjected to the following heat treatment: 2 hours at 1025°C, water cooling and 6 hours at 780°C, air cooling. The chemical composition of the test material is given in Table 1, while Table 2 shows the physical properties and the mechanical properties as a function of temperature. The micrography of Figure 1 shows the microstructure of the batch of the material under investigation in the initial state.

Table 1 Chemical composition of Inconel 718 (wt%).

C	Si	Mn	P	S	Cr	Mo	Ni	Al	B
0.032	0.16	0.1	0.006	0.001	17.26	2.98	50.86	0.55	0.003

Co	Cu	Nb	Ti	Se	Ta	Fe	Pb	Bi
0.08	0.03	5.15	1.03	1ppm	0.007	bal.	1ppm	3ppm

Table 2 Mechanical properties of Inconel 718.

	E [GPa]	ν	σ_y [MPa]	σ_U [MPa]
T=25°C	200	0.294	1090	1270
T=687°C	165	0.292	950	1100

3. SPECIMEN AND TEST DESCRIPTION

Cylindrical test specimens for creep tests with the geometry shown in Figure 2 (left) have been obtained from the material previously described. The specimens present threaded ends to connect them to the rods that impose the load, as well as two collars to place the extensometer; they are characterised by a useful section of 25 mm and by a diameter of 5 mm. The size of the specimens has been set considering the material availability. To examine the dependence of the creep behaviour of the material on the processing direction of the bar, cylindrical test-pieces were extracted oriented both longitudinally and transversely (see Figure 2 (right)). The experimental uniaxial creep tests were carried out at constant load according to ASTM standards [15]. The first set of tests consisted of fixing the temperature and varying the nominal applied stress. The nominal stress, assumed as the initial applied stress, ranged approximately from 500 MPa to 600 MPa, and the temperature was set as 687ºC.

The second set of tests consisted of fixing the nominal stress value and varying the test temperature. The nominal stress was set at 555 MPa, and the temperature ranged between 667°C and 707°C.

The tests were carried out on a SATEC machine that enables a maximum load of 50 kN, with a leverage

ratio of 20:1. The oven, model SF-17, has a cylindrical form and opens longitudinally. It is divided into three zones, by which temperature may be controlled separately. The maximum allowed test temperature is 1200°C, controlled with type K thermocouples (Chromel/Alumel). Three type S thermocouples (Platinum/Platinum 10% Rhodium with mineral oxide insulation and Inconel sheath) were placed respectively in the upper, central, and lower part of the specimen gauge length. The oven, the SATEC machine, and the specimen with thermocouples and the extensometers are shown in Figure 3 (left).

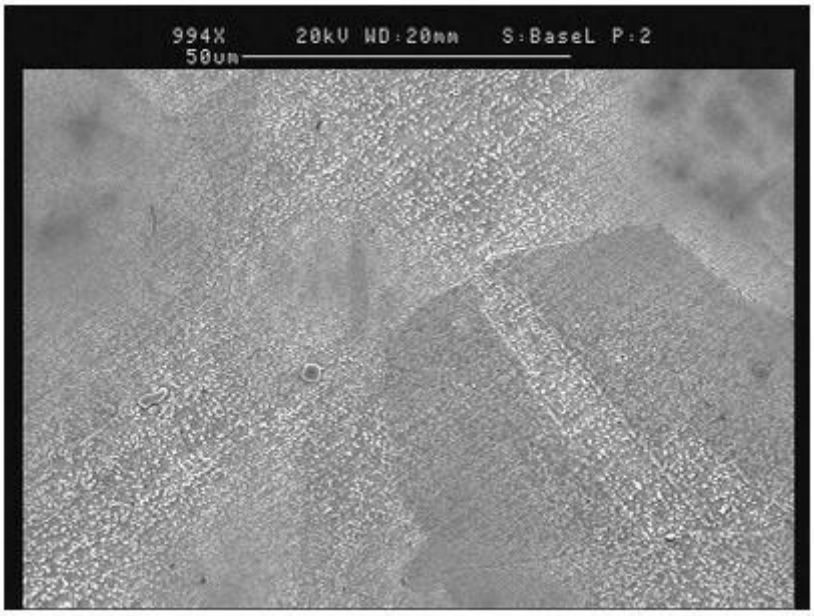

Figure 1 Microstructure of Inconel 718 in the initial state, SEM image.

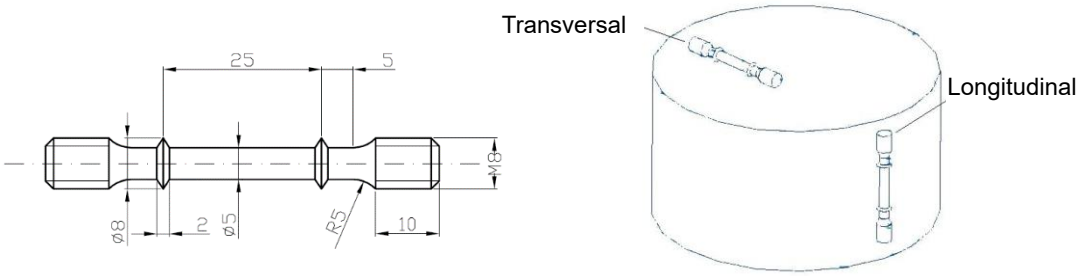

Figure 2 Geometry of tested specimen (left) and placement of longitudinal and transversal specimen (right).

The tests were carried out with initial stresses between 490 and 610 MPa and three temperature levels of 667, 687, and 707°C. The temperature control of each S thermocouple on the specimen was +-1°C, and the elongation of the specimen was measured with a LVDT, RT-214, with a calibrated measuring range of +-1 mm and a tolerance range between +-1 μm and +-5 μm.

Firstly, the linearity in the response of the LVDT during cold loading and unloading was checked. After that, the temperature transient started. As an example, the temperature transient is given in Figure 3(right) for the test at 707°C. The temperature was increased gradually in two phases with a total duration of 3 h for all tests. The first phase consisted of a ramp that varied from 0 to 680ºC and a waiting time of 0.5 h. The second phase consisted of a ramp that varied from 680 to 707°C with a final waiting time of 0.5 h. At the end of the temperature transient, the load was applied and then the test was carried out. The measurements were taken at 667ºC, 687º C and 707ºC. The data were acquired using a HEWLETT PACKARD HP 34970A multimeter and then processed by a program created specifically in MATLAB environment to save the final experimental data for each test.

4. UNIAXIAL CREEP BEHAVIOUR

The creep strain (ε) and the relative trend of the creep strain rate as a function of time (t) are presented for the first set of tests with the initial stress varying for a fixed value of the test temperature, and for the second

set of tests with the test temperature varying, for a fixed value of the initial stress.

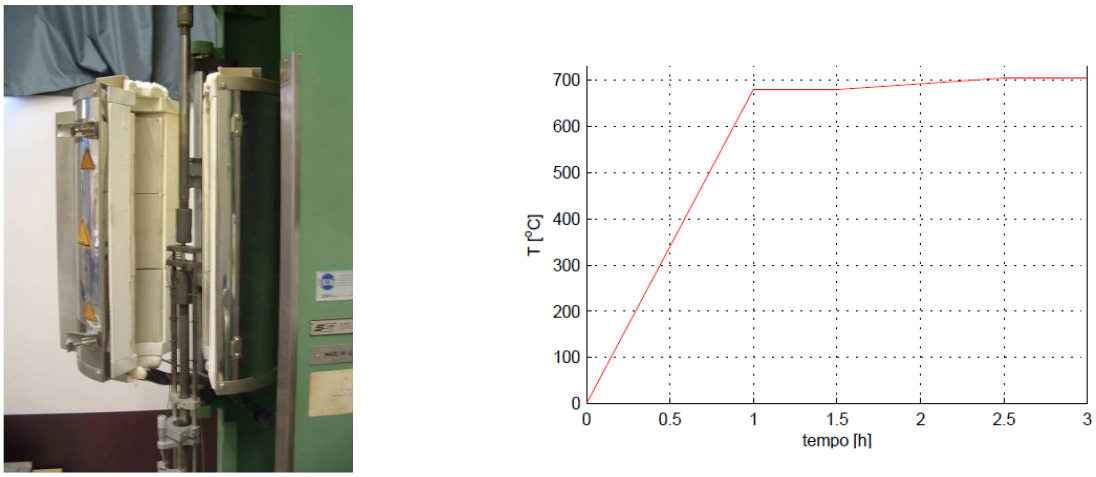

Figure 3 SATEC machine with the specimen placed inside the oven (left). Temperature transient for test at 707°C measured by the S thermocouple placed at the central part of the specimen gauge length (right).

Creep curves for experimental tests performed on specimens along the longitudinal and transversal directions, varying the nominal stress at the temperature of 687°C, are presented in Figure 4. The Inconel 718 superalloy showed the typical creep behaviour, with the presence of the three creep stages, i.e. transient, steady-state and tertiary stages. In both longitudinal and transversal directions, the primary and secondary creep phases have a reduced extension in comparison to the tertiary creep phase. It is important to notice that this behaviour is not valid for pure metals, for which the primary and secondary phases represent a greater percentage of the test specimen's lifetime. The limited extent of the secondary creep period can be demonstrated very effectively by plotting the creep rate as a function of time, as shown in Figure 5. From these figures, it is evident the decrease in the rupture time as the applied initial stress increases. What is not noticeable, however, is a monotonous trend of the strain at rupture as a function of the applied nominal stress.

Some tests were carried out for longitudinal and transversal test specimens subjected to the same nominal stress level and temperature equal to 687ºC, to compare their responses. These tests were performed with a nominal stress value of 600 MPa, 555 MPa, and 543 MPa. For σ=600 MPa and σ=555 MPa; the longitudinal specimens show a higher initial deformation than the transversal ones. However, the latter presents a final strain lower than that of the longitudinal specimen. For σ=543 MPa, the results differ from the previous one. In this case, the transversal specimen shows a higher initial deformation and final strain than the longitudinal one.

The results presented are for very short duration creep tests. The observed mechanisms are relevant for practical applications when the presence of a notch or a crack must be considered.

Creep tests were carried out at three temperature levels, 667ºC, 687ºC and 707ºC, for longitudinal specimens only. No tests have been carried out with varying temperatures in the transverse direction. The nominal stress value was fixed at 555 MPa. Creep curves and the strain rate as a function of time are presented in Figure 6 (left). As expected, with the temperature rise, a shortening of the transient stage was found, as well as an increase in the strain rate in the secondary stage and a reduction in the rupture time. This behaviour is most noticeable during the transition from 687°C to 707°C. The limited extent of the secondary creep period, highlighted by plotting the creep rate as a function of time (Figure 6 right), is confirmed at the three levels of temperature which have been investigated. In addition, also in this case, a monotonous trend of the strain at rupture as a function of the temperature is not noticeable.

The duration of each creep stage, by varying the initial stress level, is summarised in Table 3 for tests at different nominal stress values and temperature equal to 687°C. For the longitudinal direction, the primary stage duration in percentage lies between 5.7 and 7.4% for stresses ranging from 512 to 600 MPa. The secondary stage duration lies between 7.4 and 31.9%, while the tertiary stage duration is always higher than 70%, except for the test with a nominal stress value of 512 MPa. It is presumed that this level of stress produces a different response in terms of creep mechanism.

Also, for the transversal direction, as can be seen in Table 4, the tertiary stage is dominant in the response with a duration in percentage higher than 70%, except for the test with an initial stress value of 494 MPa,

possibly leading to a different response in terms of creep mechanism as before. It is worth mentioning that, at comparable stress levels, creep curves in the longitudinal direction give a higher creep strain rate and a higher rupture time than the corresponding ones in the transversal direction.

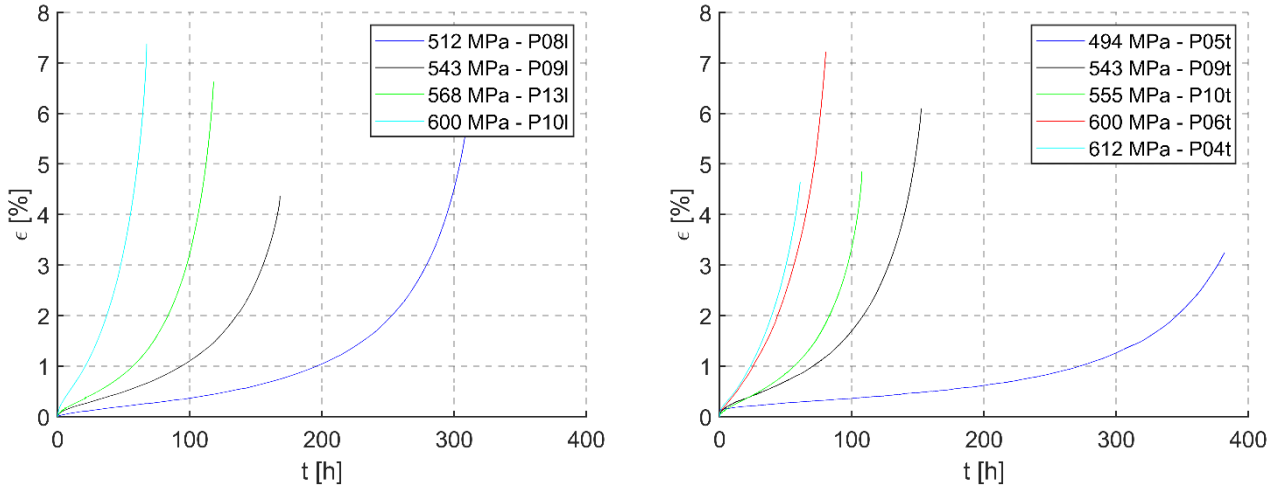

Figure 4 Creep curves for longitudinal (left) and transversal direction (right), varying the nominal applied stress, at 687°C.

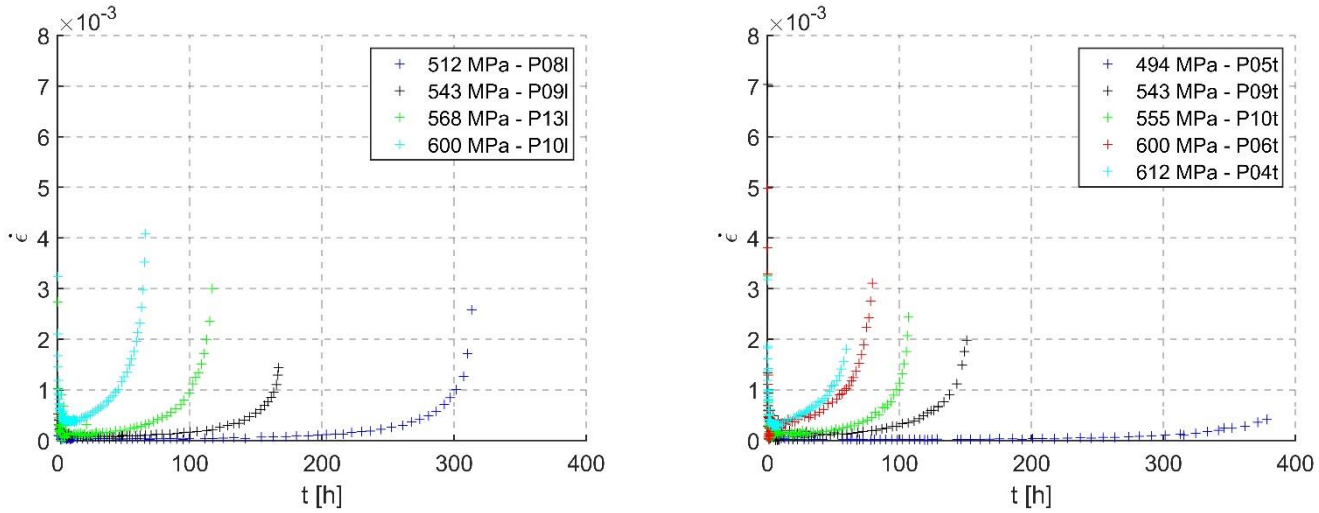

Figure 5 Strain rate as function of time along longitudinal (left) and transversal direction (right), direction, varying the nominal applied stress, at 687°C.

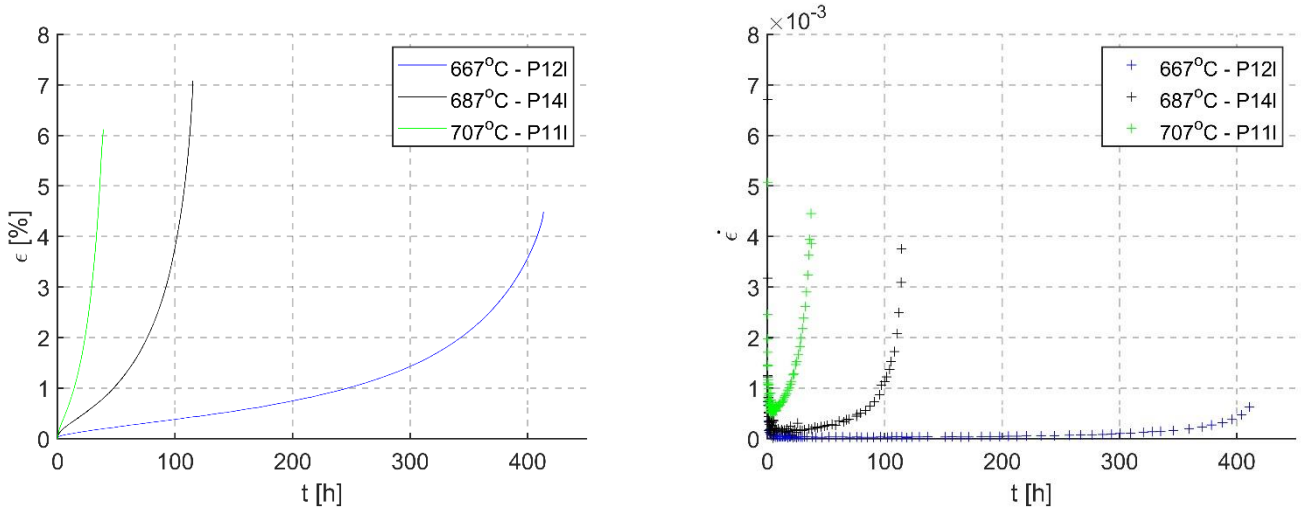

Figure 6 Creep curves (left) and strain rate as a function of time (right), at 555 MPa and varying the temperature.

Table 5 shows the duration of each creep stage, varying the temperature for a fixed nominal stress value of 555 MPa. For temperatures ranging from 667 to 707°C, the primary stage duration in percentage ranges between

7.0 and 8.5%. The secondary stage duration lies between 13.2 and 26.6%, while the tertiary stage duration is always higher than 60%. If temperatures increase, the duration of the tertiary stage also increases.

Table 3 Duration of each creep stage for creep tests along the longitudinal direction, with varying nominal stress and fixed temperature.

Test	Initial stress [MPa]	T [°C]	t_R [h]	Primary stage duration [%]	Secondary stage duration [%]	Tertiary stage duration [%]
P08l	512	687	313	6.4	31.9	61.7
P09l	543	687	168	5.9	23.8	70.3
P13l	568	687	118	5.9	19.4	74.7
P10l	600	687	67	7.4	7.4	85.2

Table 4 Duration of each creep stage for creep tests along the transversal direction, with varying nominal stress and fixed temperature.

Test	Initial stress [MPa]	T [°C]	t_R [h]	Primary stage duration [%]	Secondary stage duration [%]	Tertiary stage duration [%]
P05t	494	687	384	13.0	23.4	63.6
P09t	543	687	152	5.2	23.0	71.8
P10t	555	687	107	5.7	17.1	77.1
P06t	600	687	80	2.5	16.1	81.4
P04t	612	687	61	3.3	13.1	83.6

Table 5 Duration of each creep stage for creep tests along the longitudinal direction with varying temperature and fixed nominal stress.

Test	Initial stress [MPa]	T [°C]	t_R [h]	Primary stage duration [%]	Secondary stage duration [%]	Tertiary stage duration [%]
P12l	555	667	413.6	8.5	26.6	64.9
P14l	555	687	115.1	5.7	17.2	77.1
P11l	555	707	38.8	7.0	13.6	79.4

In Inconel 718 superalloy, as in most of the engineering alloys used in power generation and propulsion, creep strength is derived from the presence of precipitate particles dispersed within the matrix. These dispersions are unstable with respect to time and temperature. The intrinsic instability of the particle-microstructure has led, initially, to the suggestion that this is the main cause of the extended period of tertiary creep illustrated before. However, Dyson and McLean [3] have already demonstrated that this intuitive view does not stand up to quantitative scrutiny for nickel-based superalloys. Basically, the shape of the creep curve in these alloys is primarily a function of strain rather than time or temperature, and it is compatible with a dislocation sub-structure that is unstable to deformation. Moreover, Dyson and Gibbons in [16], analysing experimental data from a variety of sources and recent studies about the correlation between creep behaviour and microstructure evolution, indicate that the rate at which tertiary creep strain accumulates in nickel-based superalloy is dependent on creep strain at fracture (ductility). When the ductility is about 10%, the intrinsic instability to strain of the dislocation substructure (strain-softening) is dominant. When ductility is low, less than 2%, the rate of evolution of grain boundary cavitation is sufficiently high for it to be the primary cause of creep acceleration.

Adopting a similar procedure to that used in [16], the creep rates at increasing strains in the tertiary creep stage were normalised to the secondary creep rate. Results for the experimental tests carried out in this work are reported in Figure 7 for the longitudinal direction and the transversal direction at different levels of the nominal stress and temperature equal to 687°C, and in Figure 8 for tests at different temperatures and nominal stress equal to 555 MPa. A significant feature is that the increase rate of $\dot{\varepsilon}_{tertiary}/\dot{\varepsilon}_s$ with creep strain is highly dependent on the rupture ductility of the material. Rapid increase of $\dot{\varepsilon}_{tertiary}/\dot{\varepsilon}_s$ with strain is associated with low ductility at failure in creep. Creep ductility results in a critical parameter influencing the rate at which tertiary creep develops in the examined alloy, and it is lower in the transversal direction than in the longitudinal direction. However, Figure 7 shows an anomalous behaviour in the response of the specimen subjected to the stress σ = 512 MPa, probably because, as mentioned, this stress level is low if compared to the others and different creep mechanisms activated.

The results obtained in the present paper are confirmed by the studies reported in [16] which, in the case of titanium and aluminium or with niobium and aluminium reinforced alloys, showed similar trends. Also in [4], tests were carried out on nickel-based superalloys of slightly different compositions and no systematic trend

was found depending on the volume fraction of the precipitates. In alloys reinforced with titanium and aluminium or with niobium and aluminium, when the material with coarse crystals has a greater volume fraction of precipitates and less ductility, it has a rapid increase of the parameter $\dot{\varepsilon}_{tertiary}/\dot{\varepsilon}_s$ as deformation increases. However, more ductile materials have a smaller increase of the previous parameter, and this growth is less variable with the increase of the fraction of the precipitates and with the variation of the parameter, which expresses the mismatch of the lattice. From these considerations, it should be concluded that the rate of accumulation of the tertiary creep strain is more influenced by the rupture ductility than by the microstructure. As the ductility decreases, the strain accumulation rate of the tertiary creep increases. More recently, the dominant position of the tertiary region in the creep curve of Inconel 718 alloy, and its correlation with a creep fracture characteristic governed by creep voids formation and fracture ductility, have been confirmed by the experimental work reported in [17,18].

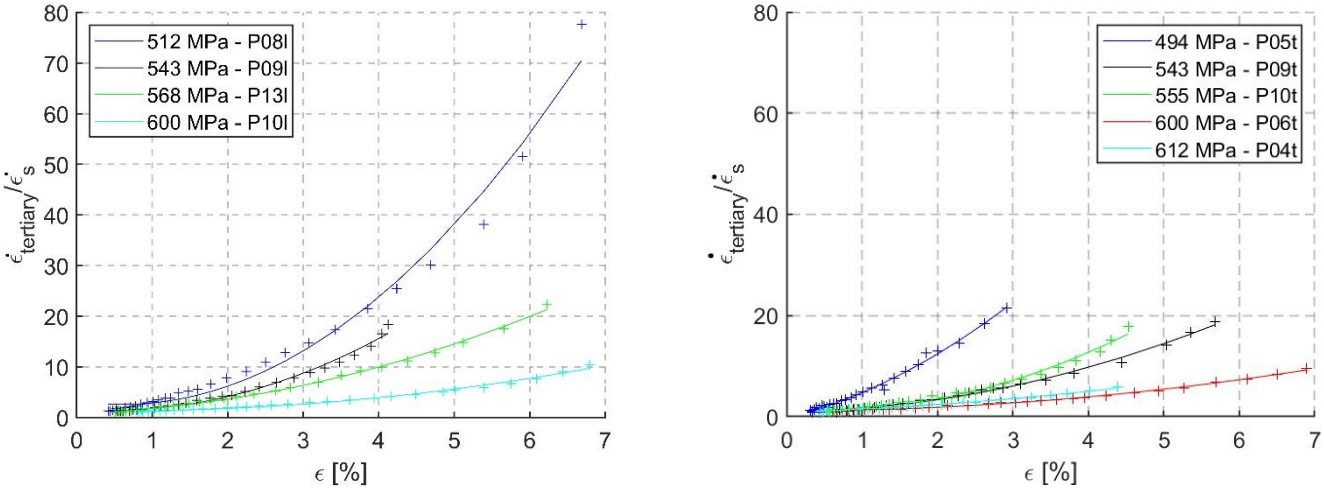

Figure 7 Rate of acceleration of tertiary creep as function of creep strain, longitudinal direction (left) and transversal direction (right) at 687°C.

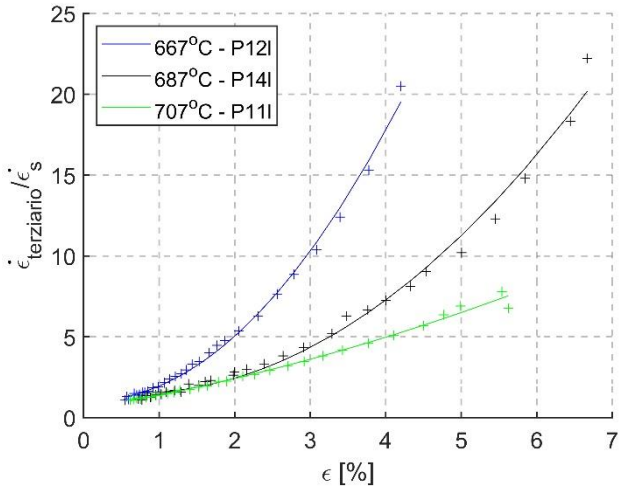

Figure 8 Rate of acceleration of tertiary creep as function of creep strain, for tests in the longitudinal direction at different values of temperature.

5. CONSTITUTIVE EQUATIONS

The availability of constitutive equations describing accumulative strain and creep rupture is an essential tool in the design and assessment of structures and components subjected to high temperatures. Moreover, the formulation and validity of given constitutive equations has considerable theoretical implications.

Simple mathematical models may not always describe the entire experimental creep curve due to the complexity of the phenomenon. Consequently, the formulation of constitutive equations that describe experimental creep generally refers to one of the individual phases: transient, steady-state, or tertiary.

Based on the experimental results presented in the previous chapters for the superalloy Inconel 718, some of the constitutive equations already developed for other materials, both for single stage of the creep curve and for the entire experimental curve, will be illustrated and discussed in the following

5.1 Transient creep

Transient creep represents the first stage of the creep curve with decreasing deformation rates. Several models have been proposed in the literature to describe the strain evolution at this stage for different stress and temperature values. Among the most well-known equations, those of Garofalo and Li should be highlighted.

Considering that microstructural changes occur during deformation, and according to the concept that the change of creep rate in transient and steady-state regions follows first-order reaction kinetics, Garofalo proposed the following strain-time relation to describe the primary and secondary creep stages [19]:

$$\varepsilon = \varepsilon_0 + \varepsilon_t[1 - \exp(-mt)] + \dot{\varepsilon}_s t \quad (1)$$

which can be rearranged as:

$$ln(\dot{\varepsilon} - \dot{\varepsilon}_s) = -mt + constant \quad (2)$$

where ε_o is the instantaneous strain on loading, ε_t is the total strain in the primary phase, m is the rate of exhaustion of transient creep and $\dot{\varepsilon_s}$ is the nominal steady-state creep rate.

Li's equation also predicts a relationship between the magnitude of primary creep strain and the steady state creep rate, although if the multiplication of dislocations, which occurs in the primary phase, follows a first-order kinetic reaction, while their exhaustion (immobilisation) follows a second-order kinetic reaction.

Li's equation [19] can be written as:

$$\varepsilon = \varepsilon_0 + \frac{\dot{\varepsilon}_s}{K_1} ln\left[1 + \frac{\dot{\varepsilon}_i - \dot{\varepsilon}_s}{\dot{\varepsilon}_s}(1 - \exp(-K_1 t))\right] + \dot{\varepsilon}_s t \quad (3)$$

where ε_o is the instantaneous strain on loading, K_1 is the dislocations multiplication rate constant, $\dot{\varepsilon_i}$ is the initial strain rate, and $\dot{\varepsilon_s}$ is the nominal steady-state creep rate.

Equation (3) can be rearranged as:

$$ln\left(1 - \frac{\dot{\varepsilon}_s}{\dot{\varepsilon}}\right) = -K_1 t + constant \quad (4)$$

Many experimental works in the literature have demonstrated that the Garofalo and the Li equations approximate very well the trend of the primary and secondary phases in the case of pure metals and in that of alloys of one or more phases [20, 21].

Experimental data of the transient stage for tests presented in Section 2 were arranged in the form of (t, $\ln(\dot{\varepsilon} - \dot{\varepsilon_s})$) and ($t$, $1 - \dot{\varepsilon_s}/\dot{\varepsilon}$) to assess the validity the applicability of Garofalo's and Li's equations, respectively, for transient and steady state creep of the investigated alloy, according to Equation (2) and (4). In both cases the considered model can be considered valid if a linear trend is obtained from the regression analysis of the experimental data plotted with these criteria. Figure 9 (left) shows the experimental data plotted as $\ln(\dot{\varepsilon} - \dot{\varepsilon_s})$ vs time for the longitudinal tests, varying the nominal applied stress (Figure 4). Regression analysis based on ordinary least squares method has shown that a linear predictor fit is not applicable; rather a parabolic fit must be considered. The meaning of these results is that the Garofalo model cannot be regarded as valid to represent the considered set of the experimental data, and to reproduce the behaviour of the transient and steady state creep in the longitudinal direction of the examined alloy, varying the applied initial stress. Figure 9 (right) reports the same experimental data of longitudinal tests, obtained varying the nominal applied stress plotted as $ln(1 - \dot{\varepsilon_s}/\dot{\varepsilon})$ versus time. In this case, regression analysis based on ordinary least squares method has shown that using a linear predictor fit, and then the Li's equation, the results are valid to represent the considered set of the experimental data, and to reproduce the behaviour of the transient and steady state creep in the longitudinal direction of the examined alloy, varying the applied initial stress. Figure 10 shows the same comparison for the transversal tests performed varying the nominal applied stress. For the superalloy under study, the applicability of the Li model was confirmed also for transversal tests, while the Garofalo model also in this case turned out to be not valid. For the sake of completeness, the experimental data for longitudinal specimens were compared with Garofalo's and Li's models for different temperature values (see Figure 11). Also considering tests at constant load and varying the temperature, the validity of the Li's model was confirmed, while the Garofalo model has proven not able to represent the experimental data. For all the tests, it can be observed that, for increasing time, the experimental points were less concentrated around the straight line in Li's model. This higher experimental scatter may be due to the progressive approach to the steady-state stage.

The slope of the linear fit in the plot $ln(1 - \dot{\varepsilon_s}/\dot{\varepsilon})$ vs time model represents the constant K_1 in Li's equation. The constant K_1, calculated for all the experimental tests in the longitudinal and transversal direction performed varying the initial stress and at constant temperature(687°C), are reported in Figure 12 as function of the nominal stress and the creep strain rate of the secondary phase, respectively. It can be noticed that these relationships are linear both for the longitudinal specimens and for the transversal ones. This suggests that the primary and secondary phases should not be considered as two separate phases, since both are governed by the

same physical phenomena. Moreover, the relationships allowed to estimate a K_1 averaged parameter for the longitudinal and transversal direction of the investigated alloy.

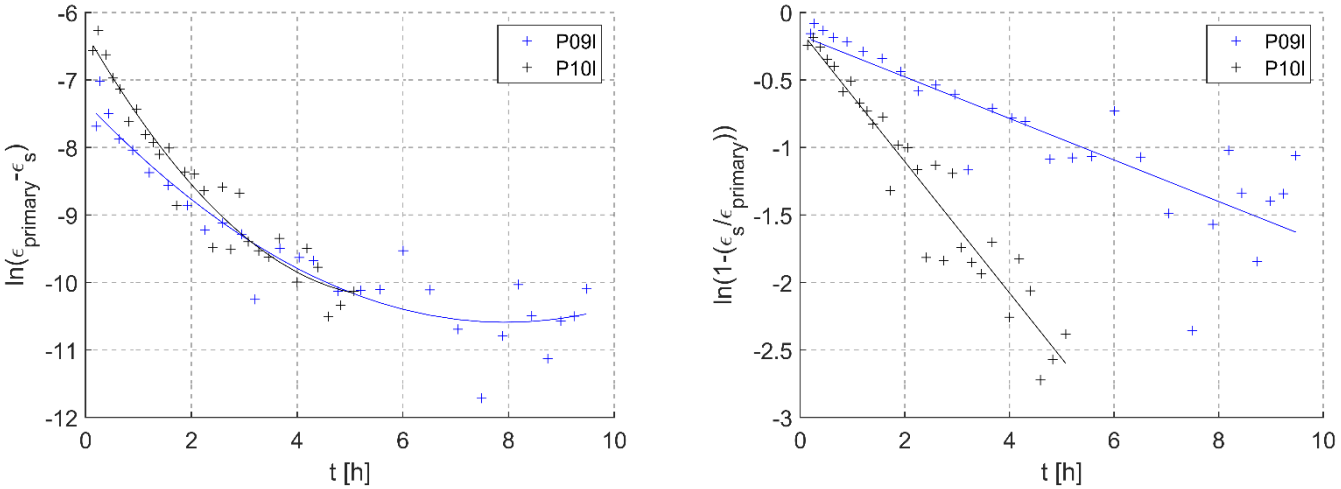

Figure 9 Comparison of the experimental data with Garofalo's model (left) and Li's model (right), for the transient creep stage, (right), for longitudinal specimens with σ=543 MPa (P09l), σ=600 MPa (P10l) and T= 687ºC.

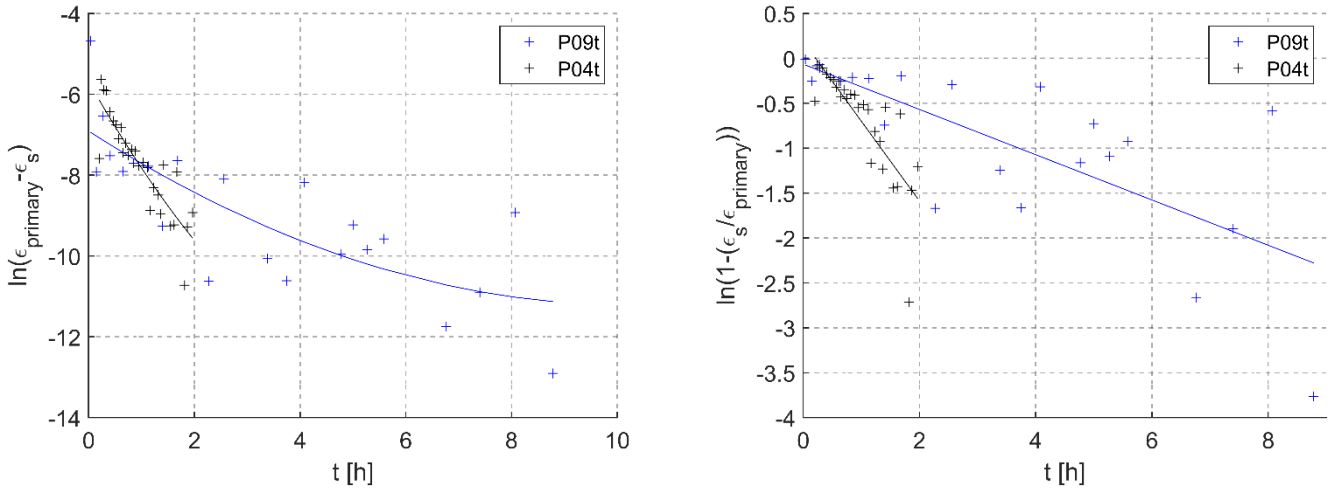

Figure 10 Comparison of the experimental data with Garofalo's model (left) and Li's model (right), for the transient creep stage, for transversal specimens with σ=543 MPa (P09t), σ=612 MPa (P04t) and T= 687ºC.

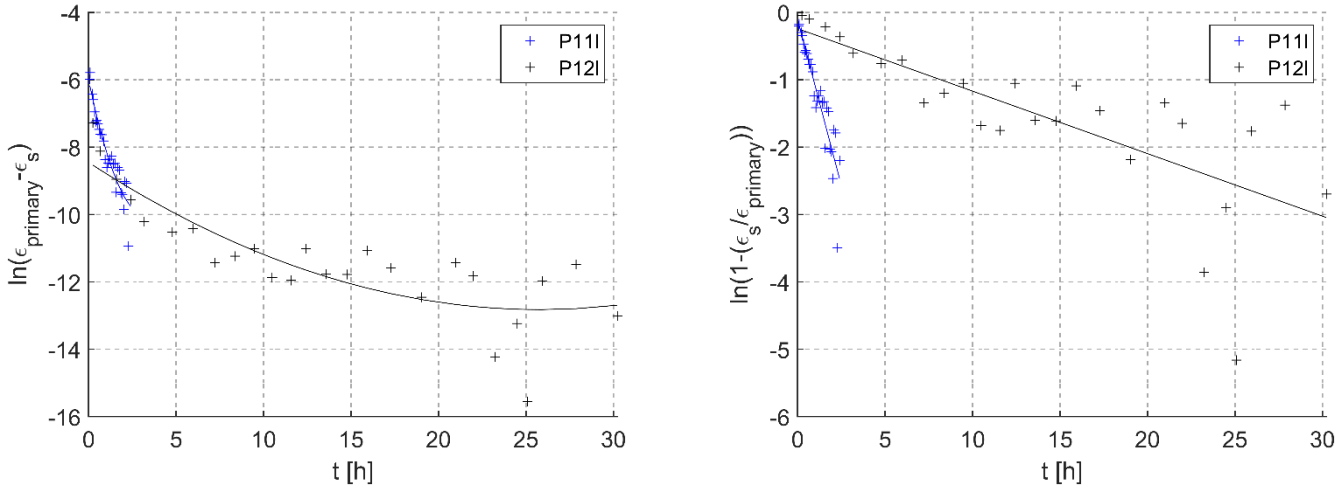

Figure 11 Comparison of the experimental data with Garofalo's model (left) and Li's model (right), for the transient creep stage, for longitudinal specimens with σ=555 MPa for T= 667º (P12l) and T= 707ºC (P11l).

Finally, Li's model was applied, assuming the averaged value of the K_1 parameter estimated for longitudinal and transversal direction, in order to reproduce the transient and steady-state stages of the experimental creep

curves (Figure 13). It can be noticed that the best fits with Li's model are the ones that showed less experimental scatter for increasing time. That is the case for longitudinal test P10l, with T = 687°C and a nominal stress equal to 600 MPa (see Figure 13 (left)) and for the test P14l, with T = 667°C and a nominal stress equal to 555 MPa (Figure 13(right)). In other cases, the experimental scatter influences the model negatively when fitting the experimental primary creep phase, the transversal specimens being the most affected ones.

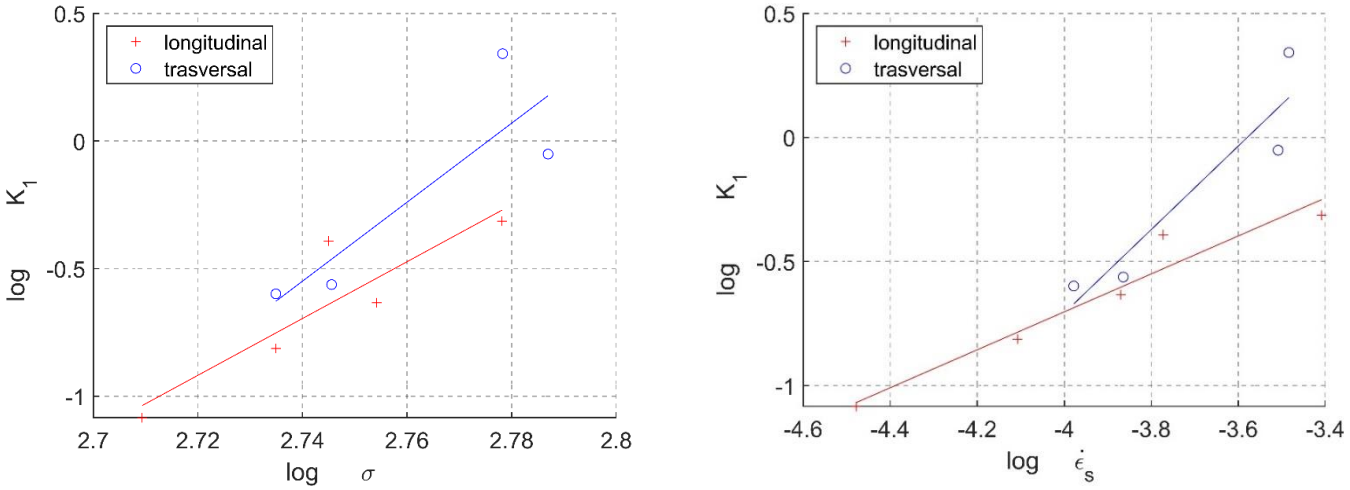

Figure 12 Constant K1 as a function of the nominal stress (left). Constant K1 as a function of the creep strain rate of the secondary phase (right) (at 687°C).

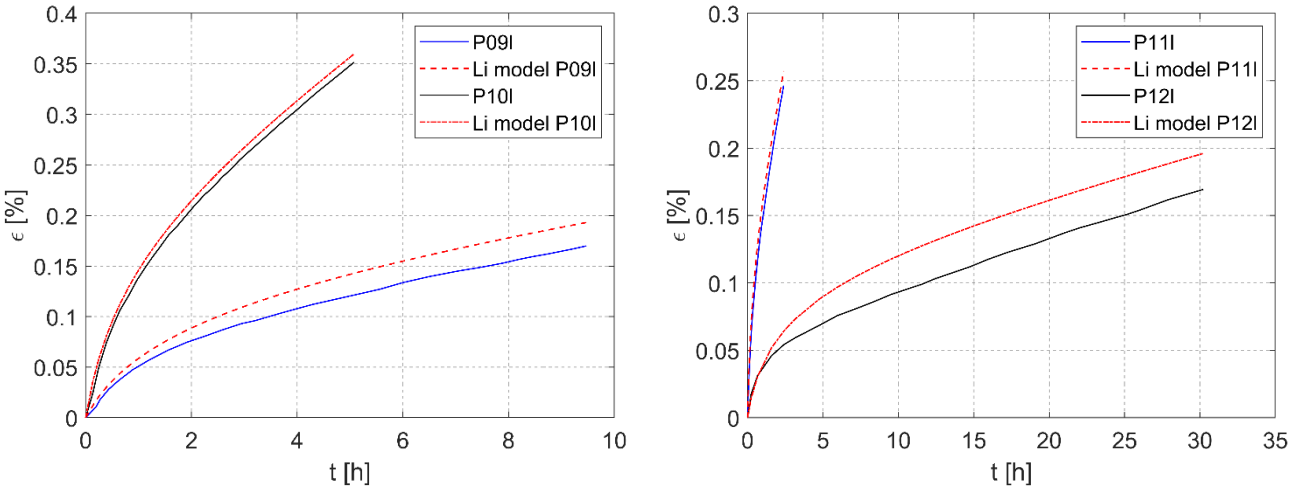

Figure 13 Comparison of the experimental data and Li's model for the primary creep phase for T= 687ºC. Longitudinal specimens with σ=543 MPa - P09l and σ=600 MPa - P10l (left). Longitudinal specimens with T=667ºC – P11l and T=707ºC – P12l (right).

5.2 Steady-state stage

The strain ε_s at the steady-state stage, which occurs at a constant strain rate, is the most studied component due to the predominance it generally has over the other stages. The most common creep constitutive law which better represents the time independence of creep rate in this stage, considering stress and temperature dependence, is based on the Norton Power Law, and the Arrhenius rate equation:

$$\dot{\varepsilon}_s = A\,\sigma^n \exp\left(-\frac{Q_c}{RT}\right) \tag{5}$$

where A is a material constant, σ is the applied stress, n is the power law exponent, Qc is the activation energy for creep, R is the gas universal constant and T is the absolute temperature.

For tests developed at a fixed temperature, the variable n can be obtained as follow:

$$n = \frac{d(log\ \dot{\varepsilon}_s)}{d(log\ \sigma)} \tag{6}$$

The creep exponent was found for the transversal and longitudinal specimens based on the experimental data, as shown in Figure 14. From the graph, it can be found that the stress exponent is 13 and 15, respectively, in the longitudinal and transversal directions. If the test is carried out at a fixed initial stress, the activation energy for creep is Qc can be obtained based on the temperature variation:

$$-\frac{Q_c}{R} = \frac{ln\,\dot{\varepsilon}_s}{d(1/T)} \tag{7}$$

The value of *Qc* equal to 547 kJ/mol was obtained, based on the experimental data for longitudinal specimens, as shown in Figure 15.

A wide variation of values of stress exponent and activation energy, mainly affected by different percentage of alloying elements and heat treatment, has been reported in the literature for this alloy in low and high stress level. Papers which investigated creep behaviour of Inconel 718 with chemical composition and heat treatment significant for the comparison have been selected. In [22], a double aging heat treatment was considered: solution treatment of 1095°C for 1.0 h/AC, aging at 955°C for 1 h/AC, aging at 720°C for 6.5 h/ FC + 720°C for 1.5 h/FC + 620°C for 8.0 h/FC. It was suggested that the controlling mechanism of creep deformation is driven by dislocation-particle interaction, controlled by the particle shearing, a value of n=11.8 was found for stress ranging between 510 MPa and 700 MPa at 675°C and, for temperature ranging between 650°C and 675°C, a value of Qc=374.3 kJ/mol for stress equal to 625 MPa and a value of Qc=956.8 kJ/mol for stress equal to 510 MPa were obtained. In [23], the material had a melting furnace VIM, VAR remelting in heat treatment, homogenization, hot forging in open die for roughing, roughing hot rolling and hot rolling finish. Relatedly severe mechanical stresses are investigated, n=36.4 for stress ranging between 700 MPa and 814 MPa at 650°C, and Qc=512.9 kJ/mol for stress equal to 750 MPa for temperature ranging between 650°C and 700°C are reported. Results presented in [17] reports n=15.1 for stress ranging between 560 MPa and 720 MPa at T=700°C. In this case, the alloy was subjected to a solution heat treatment at 982°C for 1 h, cooled in air, and aged at 788°C for 8 h, furnace cooled at a rate of 56°C/h to 704°C for 8 h, air cooled. Moreover, the correlation between stress exponent and deformation mechanism which implied that deformation mechanisms of Alloy 718 are dislocations cutting γ" phases for the considered conditions was highlighted. The superalloy Inconel 718 at the test conditions presented in this paper falls within the range of high stress and high temperature values examined in the comparison papers, which justify the parameters obtained from the present experimental studies.

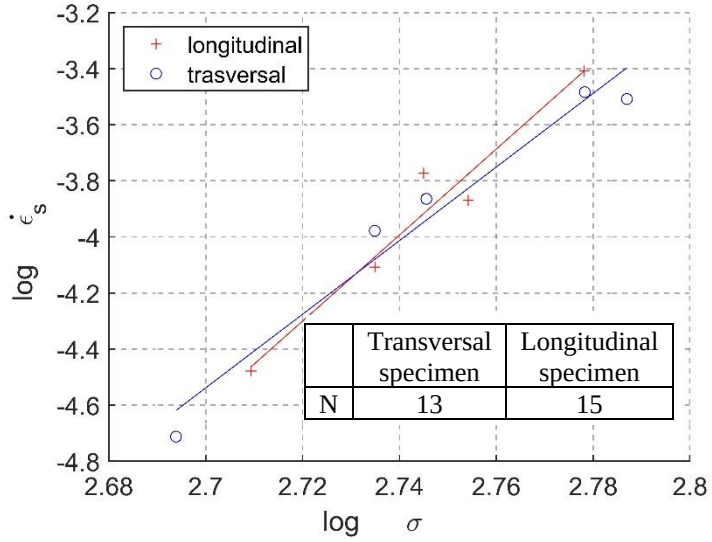

Figure 14 Logarithmic trend of the steady-state strain rate vs the logarithm of stresses.

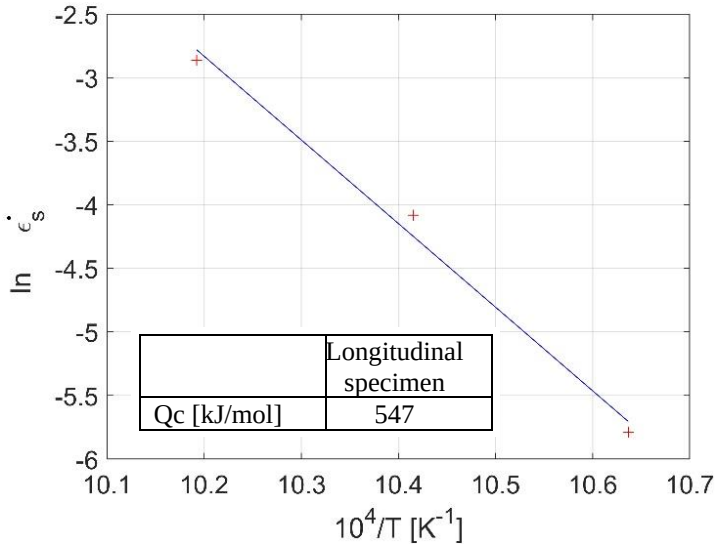

Figure 15 Logarithmic trend of the secondary strain rate vs 10^4/T.

5.3 Fracture behaviour

The acceleration on the accumulation of the strain rate, with respect to the minimum creep rate of the steady state stage, represents the beginning of the tertiary creep stage, and is the first manifestation of a possible rupture. Many metals and alloys have a linear relationship between log(t_R) and log($\dot{\varepsilon}_s$) [24]. For the material under study, the trend is shown in Figure 16, for both transversal and longitudinal specimens. The relationship between the rupture time and the strain rate of the secondary phase confirms the hypothesis that the product t_R $\dot{\varepsilon}_s$ is independent of the stress level; therefore, it is possible to use an analogous relationship to the Norton Law and Arrhenius rate equation, which was developed for the strain rate of the secondary phase.

$$t_R = A' \ \sigma^{n'} \exp\left(-\frac{Q_R}{RT}\right) \tag{8}$$

The *n'* and Q_R values depend on the stress level. The parameter *n'* for both longitudinal and transversal specimens was calculated from Figure 17, while the parameter Q_R was computed from Figure 18. The values of *n'* and Q_R are lower than the values of *n* and Q_C obtained for Equation (5). This dependence of fracture time from creep behaviour suggests that this strengthened superalloy does not exhibit the classical dislocation creep behaviour of pure metals and simple solid solution alloys. As is well-established in the literature [24, 25], the dislocation mechanism of this alloy shows strong evidence of grain boundary sliding and microtwinning.

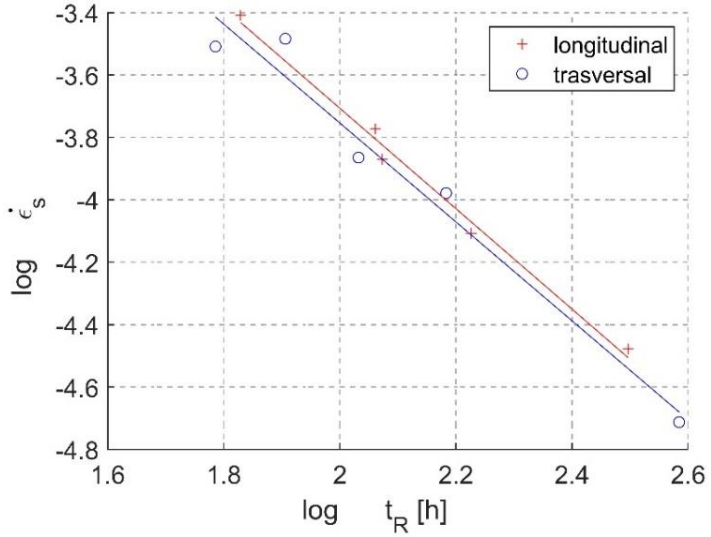

Figure 16 Logarithmic trend of secondary strain rate vs rupture time.

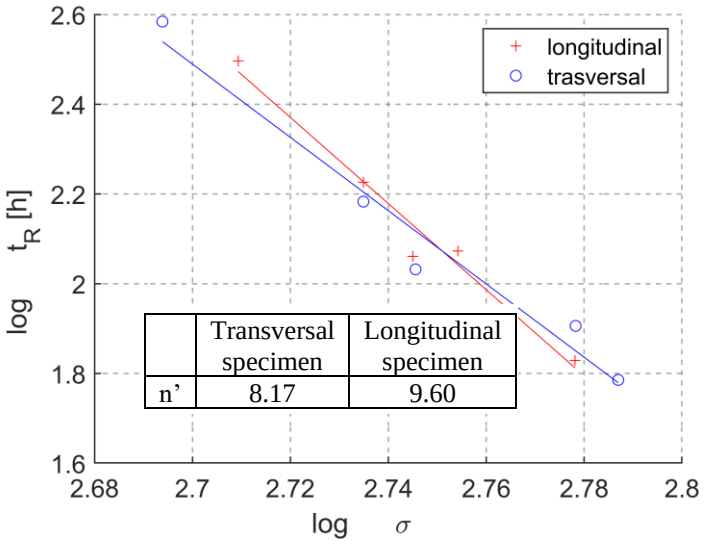

Figure 17 Logarithmic trend of the rupture time vs the logarithm of stresses.

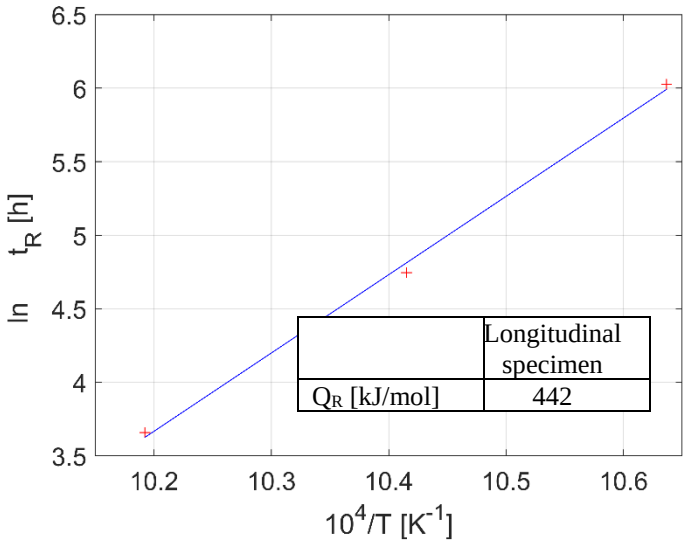

Figure 18 Logarithmic trend of the rupture time vs 10^4/T.

6. THETA PROJECTION MODEL

Creep tests are time-consuming and expensive experimental activities, and rarely allow to explore transient effects connected with start-up or shutdown of the components. Instead, the study of transient phenomena is an ideal field for computer modelling, when reliable constitutive creep equations, which describe the strain rate dependence on stress, temperature, and time, are available [26, 27].

The theta projection model was applied to fit with higher accuracy the entire creep curve of the experimental data. The model, also proposed in the main codes for high temperature assessment, describes the creep strain at a given time with the following [28]

$$\varepsilon = \theta_1(1 - \exp(-\theta_2 t)) + \theta_3(\exp(-\theta_4 t) - 1) \quad (9)$$

The first term, $\varepsilon_{pr} = \theta_1(1 - \exp(-\theta_2 t))$, represents the primary creep and defines a strain-hardening response described by an exponential decay term. The second term, $\varepsilon_{tr} = \theta_3(\exp(-\theta_4 t) - 1)$, represents the tertiary creep and defines a strain-softening response described by exponential growth.

An extension of the model was implemented by adding a linear term, in order to capture accurately the transition from the primary and the tertiary phase, accounting for secondary creep behaviour [29].

$$\varepsilon = \theta_1(1 - \exp(-\theta_2 t)) + \theta_m t + \theta_3(\exp(-\theta_4 t) - 1) \quad (10)$$

Each ϑ parameter value is estimated for each creep strain curve at a given stress and temperature by minimising the error between the experimental curve and the predicted curves. Parameters θ_1 and θ_3 are defined as *scaling parameters*, which define the extent to which the primary and tertiary phases of creep affect the creep strain accumulation. Parameters θ_2 and θ_4 are defined as *rate parameters* that define the non-linear response of the first and tertiary stages. The coefficient θ_m, responsible for the linear term in the extended equation, is defined as follows, and it is analogous to Norton's law presented in the previous paragraphs:

$$\theta_m = A\,\sigma^n \exp\left(-\frac{Q_c}{RT}\right) \quad (11)$$

Figure 19 - Figure 21 present experimental creep curves in the longitudinal and transverse directions for different initial stresses along with the theta projection model estimation. In addition, the same was performed for the tests where the stress was fixed, and the temperature varied.

Figure 22-Figure 24 report the θ coefficients obtained from the theta model simulation, plotted in function of the stress, for longitudinal and transversal specimens, and of the temperature for the longitudinal specimens with varying temperature and fixed initial stress. The values of the θ coefficients, for each experimental curve, are also reported in Table 6, Table 7, and Table 8. Normalization of the creep curves with the rupture strain (ε_f) was not carried out in this paper. For completeness, the rupture strain assumed as the final strain in the creep experimental curves of Figure 4 and Figure 5 (left) is shown in Table 6, Table 7, and Table 8.

Figure 22-Figure 24 also reports the best fit of each parameter with stress and temperature, which enables the capabilities of the model to predict accumulation of creep damage and creep ductility closely resembling those obtained experimentally. These correlations allow to set a creep material model, including transient effects, to be used in numerical approach to describe the behaviour of real components under steady-state or transient conditions across multiple isotherms and stress levels.

Moreover, the modified θ projection method has a clear analytical approach, based on the established equations (10) and (11), that make the model simple to be implemented and coupled with appropriate failure criteria.

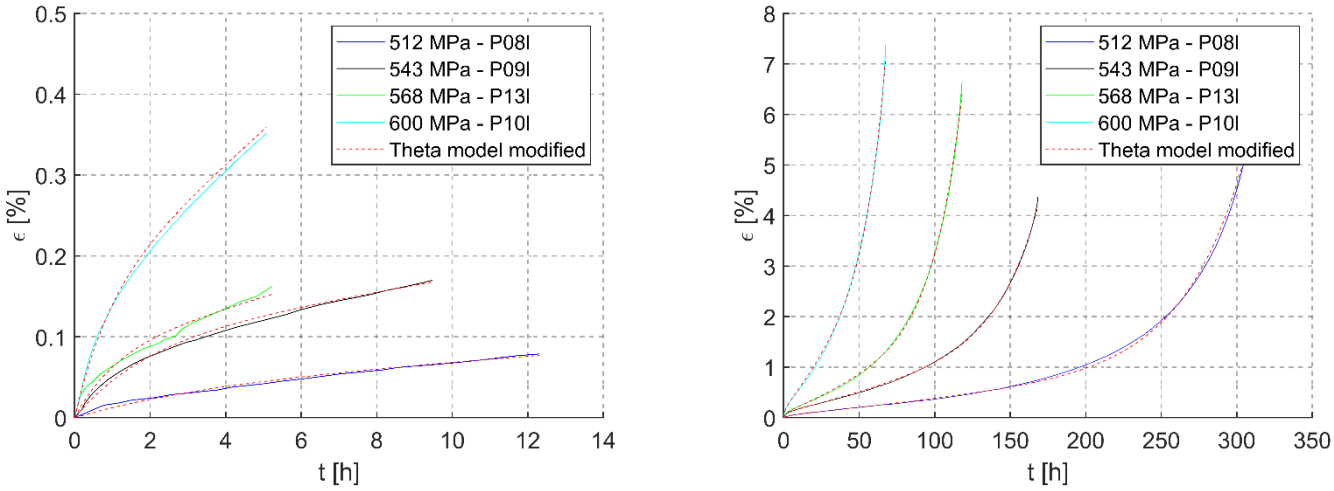

Figure 19 Comparison of the experimental data and theta's model for the primary creep phase (left) and primary, secondary and tertiary creep phases (right), for longitudinal specimens with T= 687ºC.

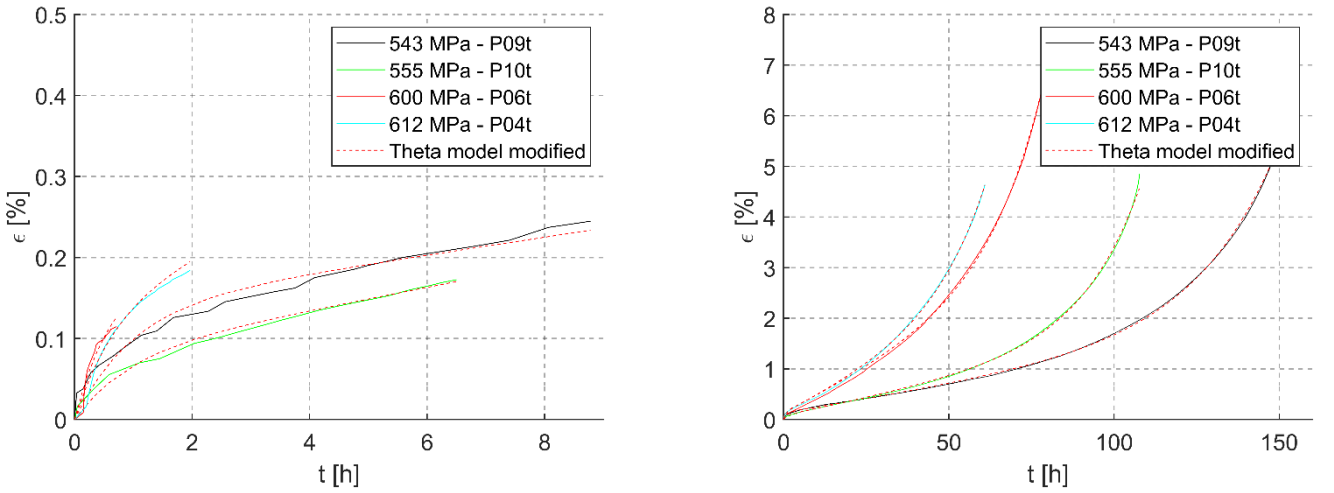

Figure 20 Comparison of the experimental data and theta's model for the primary creep phase (left) and primary, secondary and tertiary creep phases (right), for transversal specimens with T= 687ºC.

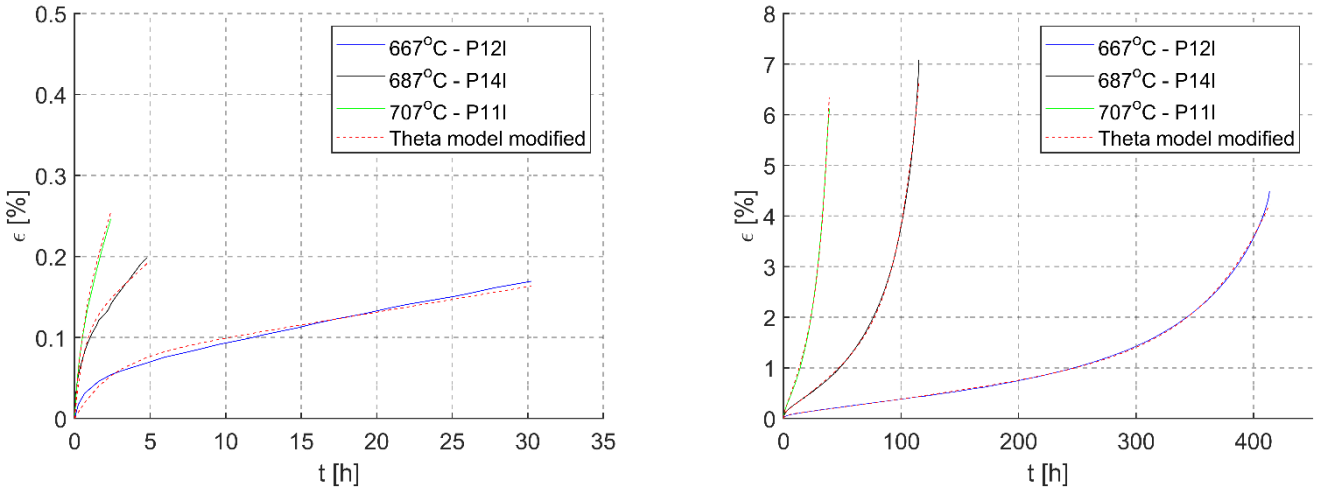

Figure 21 Comparison of the experimental data and theta's model for the primary creep phase (left) and primary, secondary, and tertiary creep phases (right), for longitudinal specimens with σ= 555 MPa and varying temperature.

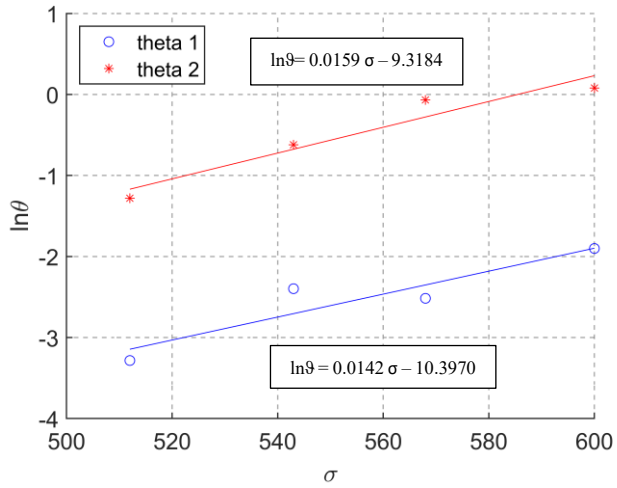

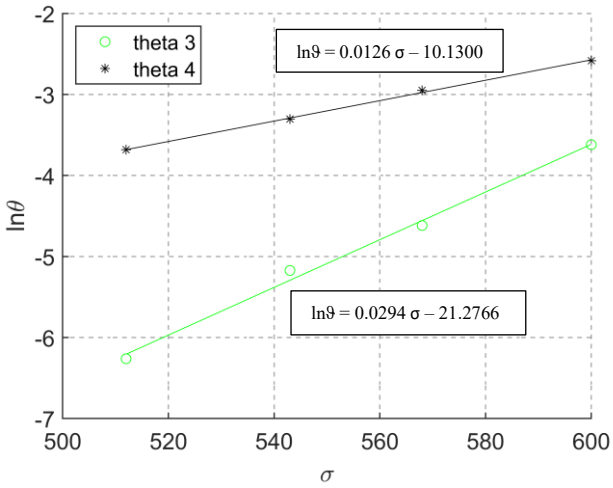

Figure 22 θ1 and θ2 coefficients (left) and θ3 and θ4 coefficients (right) for longitudinal specimens with T= 687ºC.

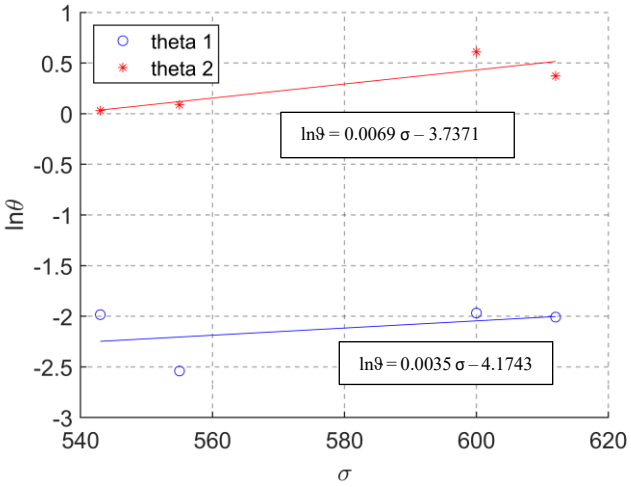

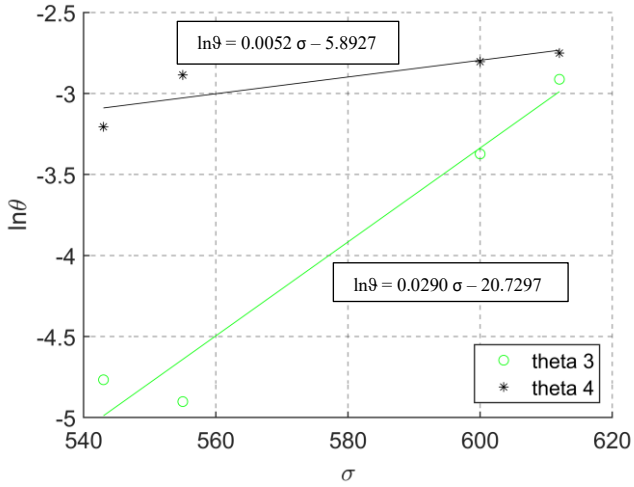

Figure 23 θ1 and θ2 coefficients (left) and θ3 and θ4 coefficients (right) for transversal specimens with T= 687ºC.

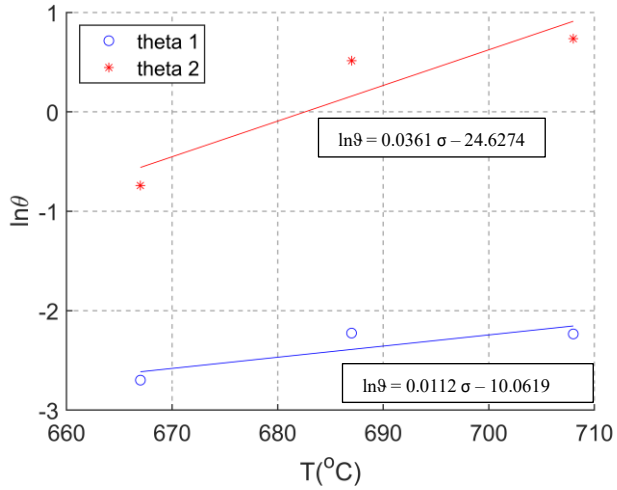

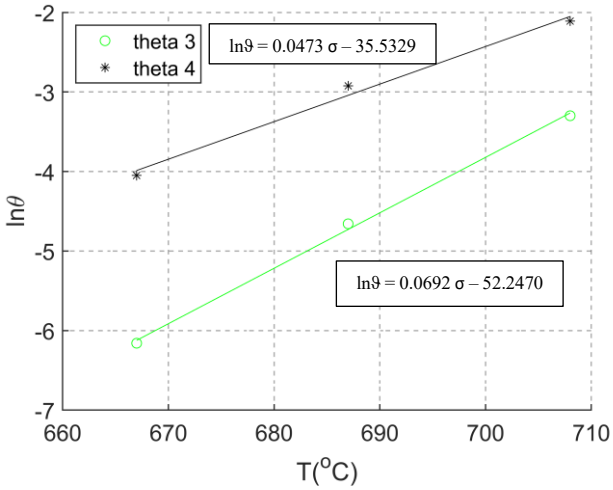

Figure 24 θ1 and θ2 coefficients (left) and θ3 and θ4 coefficients (right) for longitudinal specimens with varying temperature and σ= 555 MPa.

Table 6 θ coefficients for longitudinal specimens with T= 687ºC.

Test	Initial stress [MPa]	T [°C]	θ_1	θ_2	θ_3	θ_4	ε_f [%]
P08l	512	687	0.0375	0.2775	0.0019	0.0251	6.99
P09l	543	687	0.0910	0.5366	0.0057	0.0367	4.36
P13l	568	687	0.0808	0.9331	0.0099	0.0523	6.63
P10l	600	687	0.1495	1.0802	0.0269	0.0754	7.38

Table 7 θ coefficients for transversal specimens with T= 687ºC.

Test	Initial stress [MPa]	T [°C]	θ_1	θ_2	θ_3	θ_4	ε_f [%]
P09t	543	687	0.1375	1.0131	0.0085	0.0405	6.10
P10t	555	687	0.0788	1.0927	0.0074	0.0558	4.85
P06t	600	687	0.1397	1.8421	0.0343	0.0606	7.22
P04t	612	687	0.1342	1.4526	0.0543	0.0639	4.64

Table 8 θ coefficients for longitudinal specimens with varying temperature and σ= 555 MPa.

Test	Initial stress [MPa]	T [°C]	θ_1	θ_2	θ_3	θ_4	ε_f [%]
P12l	555	667	0.0675	0.4718	0.0022	0.0174	4.49
P14l	555	687	0.1081	1.6721	0.0095	0.0537	7.08
P11l	555	707	0.1071	2.0891	0.0369	0.1213	6.12

7. CONCLUSIONS

This paper presents the results of uniaxial creep tests conducted on Inconel 718 at various stress levels, at different temperatures, and on specimens with different orientations with respect to the processing direction of the material. The experimental data were analysed, compared, and presented in the form of creep strain curves and creep strain rates. In addition, it was focused on the creep stages such as primary, secondary, and tertiary, with particular attention on their duration and contribution to the response in terms of deformation. It has been observed that the primary and the secondary stages have a reduced extension compared to that of the tertiary one, which extends for almost the whole life until rupture. There was also a decrease in the rupture time and an increase in the deformation rate as the initial stress applied increased. Regarding the tertiary creep phase, it was found that ductility is the parameter that governed the rate of accumulated strain: the lower the ductility, the higher the rate at which strain accumulates.

The analysis of tests carried out at the same initial stress and temperature, and with a different specimen orientation with respect to the direction of processing of the material, led to conclude that the creep resistance of longitudinal specimens was greater than that of transverse specimens.

Moreover, constitutive models were applied to the different creep phases and several useful coefficients for their application were derived from the experimental data. For the primary phase, the Garofalo and Li models were applied. According to what has already been documented in literature, the experimental data followed the Li model satisfactorily. Regarding the secondary creep phase, the activation energy and the creep exponent of Norton's law have been obtained from the experimental data. The tertiary phase was also studied, and the main parameters for its characterisation were derived. Finally, the modified theta model coefficients were estimated to fit the entire creep strain curve of the experimental data; the model provides reliable constitutive creep equations for numerical study of transient phenomena in components under service conditions.

.

REFERENCES

[1] M. Durand-Charre. *The Microstructure of Superalloys*. Gordon and Breach Science Publishers, 1997.

[2] Hongjun Zhang, Chong Li, Qianying Guo, Zongqing Ma, Huijun Li and Yongchang Liu, "Improving creep resistance of nickel-based superalloy Inconel 718 by tailoring gamma double prime variants", *Scripta Materialia*, 164, 66–70, 2019.

[3] P. Maj, B. Adamczyk-Cieslak, M. Slesik, J. Mizera, T. Pieja, J. Sieniawski, T. Gancarczyk and S. Dudek, "The Precipitation processes and mechanical properties of aged Inconel 718 alloy after annealing", *Archives of Metallurgy and Materials,* 62 (3), 1695-1702, 2017.

[4] B.F. Dyson and M. McLean, "Particle-Coarsening, σ_0 and Tertiary Creep", *Acta Metallurgica*, 31, 17-27, 1983.

[5] R.Y. Zhang, H.L. Qin, Z.N. Bi, J. LI, S. Paul, T.L. Lee, S.Y. Zhang, J. Zhang, and H.B. Dong, "Temperature-Dependent Misfit Stress in Gamma Double Prime Strengthened Ni-Base Superalloys", *Metallurgical and Material Transaction*, 51, 1860-1873, 2020.

[6] Katia Cristiane Gandolpho Candioto, Felipe Rocha Caliari, Danieli Aparecida Pereira Reis, Antônio Augusto Couto and Carlos Angelo Nunes, A. Öchsner and H. Altenbach (eds.), "Characterization of the Superalloy Inconel 718 After Double Aging Heat Treatment in Mechanical and Materials Engineering, of Modern Structure and Component Design", *Advanced Structured Materials*, 70, 2015, DOI 10.1007/978-3-319-19443-1_24.

[7] Nabarro, F. R. N. , Cress C. M., and Kotschy, P., The Thermodynamic Driving Force in Superalloy, Acta Materials, 44, 3189-3198, 1996.

[8] Gao M., Chen S. , Gary Harlow D. , and Wei R. P. , Preferential Coarsening of γ" Precipitates in INCONEL 718 During Creep, Metallurgical and Materials Transaction A, 27A, 3391, 1996.

[9] Hailong Qin, Zhongnan Bi, Hongyao Yu, Guang Feng, Ruiyao Zhang, Xia Guo, Hai Chi, Jinhui Du, and Ji Zhang, "Assessment of the stress-oriented precipitation hardening designed by interior residual stress during ageing in IN718 superalloy", *Materials Science and Engineering: A*, 728, 183-195, 2018.

[10] Daniel F. Paulonis and John J. Schirra, "Alloy 718 at Pratt & Whitney: Historical Perspective and Future Challenges", *Superalloys*, 13-23, 2001. [11] C. Mercera, and B. O. Soboyejow, "Micromechanisms of fatigue crack growth in a single crystal Inconel 718 nickel-based superalloy", *Materialia*.,47(9), 2727-2740, 1999.

[12] Ying Li, Jaromír Dlouhý, Jaroslav Vavřík, Jan Džugan, Pavel Konopík, Tomáš Krajňák, and Jozef Veselý, "Investigation of short-term creep properties of a coarse-grained Inconel 718 fabricated by directed energy deposition compared to traditional Inconel 718", *Materials Science and Engineering: A*, 844, 143, 2022.

[13] Ehsan Saberi, Soheil Nakhodchi, Ashkan Dargahi and Kamran Nikbin, "Predicting stress and creep life in Inconel 718 blade-disk", *Engineering Failure Analysis,* 108, 104226, 2020.

[14] Michael Rupp, Guido Dhondt, Martin Becker, Andreas Fischersworring-Bunk, Antje Rohr, Thomas Brendel and Hans-Peter Hackenberg, "A TMF crack propagation model considering time dependency and load sequence effects", *Engineering Fracture Mechanics*, 237, 107218. 2020.

[15] ASTM E 139 - 83 (Reapproved 1990). *Standard Practice for Conducting Creep, Creep-Rupture, and Stress-Rupture Tests of Metallic Materials*.

[16] B.F. Dyson and T.B. Gibbons,"Tertiary Creep in Nickel-Base Superalloys: Analysis of Experimental Data and Theoretical Synthesis", *Acta Metallurgica*, 35, 2355–2369, 1987.

[17] Tongwei Ni and Jianxin Dong, "Creep behaviors and mechanisms of Inconel718 and Allvac718plus", *Materials Science and Engineering: A*, 700, 406-415, 2017.

[18] R.W Hayes., R.R.Unocic and M. Nasrollahzadeh, “Creep Deformation of Allvac 718Plus”, *Metallurgical and Materials Transaction A*, 46A, 2015.

[19] F. Garofalo, *Fundamentals of Creep and Creep-Rupture in Metals*, New York: Macmillan, 1966.

[20] J. Shen K., Ikeda, S. Hata and H. Nakashima, “Transient Creep in High-Purity Aluminium at Ultra-Low Strain Rate and Room Temperature by Constant Stress and Changing-Stress Experiments”, *Materials Transactions*, 52(10), 1885-1889, 2010.

[21] L. Kloc, V. Sklenička, P. Dymáček and J, Plešek, “New creep constitutive equation for finite element modelling including transient effects”, *Mechanics of Materials,* 119*,* 49–55*,* 2018).

[22] F. Rocha Caliari., K. Cristiane, G. Candioto, A. A. Couto, C- A. Nunes and D. A. Pereira Reis, “Effect of Double Aging Heat Treatment on the Short-Term Creep Behavior of the Inconel 718”, *JMEPEG*) 25, 2307–2317, 2016. DOI: 10.1007/s11665-016-2051-2

[23] T. Sugahara, K. Martinolli, D. A. P., Reis. C Moura Neto, A. A. Couto, F. Piorino Neto and M.J.R. Barboza, “Creep Behavior of the Inconel 718 Superalloy”, *Materials Research*, 25, e20210280, 2022. DOI: https://doi.org/10.1590/1980-5373-MR-2021-0280

[24] Jianting Guo, D. Ranucci, E. Picco and P.M. Strocchi, “An Investigation on the Creep and Fracture Behavior of Cast Nickel-Base Superalloy IN738LC”, *Metallurgical Transactions A,* 14A, 2329–2335, 1983.

[25] K. Chen, J. Donga, Z. Yaoa, T. Nia and M. Wang, “Creep performance and damage mechanism for Allvac 718Plus superalloy”, *Materials Science and Engineering: A*, 738, 308-322, 2018.

[26] G. Maggiani, M. J. Roy, S. Colantoni, and P. J. Withers, “MAR-M-247 creep assessment through a modified theta projection model”, *Materialia*, 7, 2019.

[27] W. J., Harrison and W.J. Evans, *Application of the Theta projection method to creep modelling using Abaqus*. Swansea University, Abaqus UK Regional User Meeting, 2007.

[28] R. Evans, J. Parker, and B. Wilshire, Recent Advances in Creep and Fractures of Engineering Materials and Structures, Pineridge Press, Swansea, 1982.

[29] *Recommendation for Creep and Creep-fatigue Assessment for P91 Components.* European Commission. Joint Research Centre. Institute for Energy and Transport, 2016.

APPENDIX A: ADDITIONAL DATA

The file of experimental data for each test (Figure 4 and Figure 6 (Left)) is named “XXXMPaYYYC_Dir.dat” where XXX is the value in MPa of the nominal stress of the test, YYY is the value of the test temperature in °C, “Dir” is “Long” for Longitudinal tests and “Trans” for Transversal tests. The data in each file are organised into two columns; the first column reports the time in [h], the second column reports the creep deformation in [%].